Proceedings of the ASME 2020
International Design Engineering Technical Conferences and
Computers and Information in Engineering Conference
IDETC/CIE2021
August 17-20, 2021, Virtual, Online

DETC2021-71552

TELEOPERATION INTERFACE FOR SAFAM, A SOLID ARTICULATED FOUR AXES MICROROBOT

Moath Alqatamin[1], Brooke Ritz, Andriy Sherehiy, Douglas Jackson, Ruoshi Zhang, Sri S Chowdhury, Danming Wei, Dan O. Popa
Louisville Automation and Robotic Research Institute (LARRI),
University of Louisville, Louisville, Kentucky, USA

ABSTRACT

The sAFAM is a novel mm-size microrobot built using MicroElectroMechanical Systems (MEMS) technology. It consists of a monolithically fabricated microrobotic arm assembled onto four in-plane actuators, capable of moving along four degrees of freedom, including translational movement in X and Y axes as well as pitch and yaw. In this paper, several design modifications were proposed to increase movement precision, stability, and controllability to the sAFAM tip. An interface is developed to assist a human operator accurately position the microrobot tip during nano-object handling. A Python-based graphical user interface (GUI) was programmed to make it intuitive for an operator to use and obtain required tip precision under a microscope. Experimental results demonstrate the functionality of the proposed control solution, and the tip motion resolution using microscope images of the microrobot tip under 20x magnification during operation. The hardware and software requirements for the proposed experimental setup and control platform are discussed in detail.

Keywords: Control, microrobotics, nano/microtechnology.

1. INTRODUCTION

Manipulation of micro-nano scale objects in a precise, controlled, and repeatable way has been a major obstacle in the field of nanotechnology. While piezo-based nano-positioners offer excellent resolution and repeatability, they are often bulky and unsuitable in limited workspace [1, 2]. Microscopic robots and robotic arms, capable of moving in multiple degrees of freedom, with sufficient range of motion could ameliorate this problem significantly. Many ideas of microscopic robots [2-7] have been developed and demonstrated over the last decade by utilizing solar, laser, piezo, magnetic and ultrasonic energy as the source of actuation. Over time the manipulation precision of these microrobotic tools has increased, while size of these robotic structures has continuously decreased [8, 9]. Fabrication process of such microrobots has many challenges. Microelectromechanical systems (MEMS) technology has been a key solution for fabrication of microrobot components [10, 11] and development of automated microscale devices, for in-situ probing of nano/microscopic objects inside the Scanning Elctron Microscope (SEM) [12, 13]. Tsui and Geisberger in [14, 15] have proposed snap-fastener style MEMS coupled devices via microassembly, also known as the Zyvex connector. This connector makes it possible to build microrobot arms capable of 3D positioning by using 2 ½ D MEMS components fabricated on a plane Silicon wafer.

The articulated four axes microrobot (AFAM) has been first proposed by Murthy et al [16] by taking advantage of the Zyvex connector implemented in a $\mathbf{100}\ \mu\boldsymbol{m}$ thick Silicon on Insulator (SOI) wafer using MEMS technology. The workspace of AFAM [17] was measured to be $\mathbf{50}\boldsymbol{\mu m} \times \mathbf{50}\boldsymbol{\mu m}$ for translational motion in $\boldsymbol{X}$ and $\boldsymbol{Y}$ directions and $\mathbf{70}\boldsymbol{\mu m}$ in the Z direction corresponding with the robot pitch. The footprint of this robot was smaller than $\mathbf{3}\boldsymbol{mm\ x}\ \mathbf{1.5}\boldsymbol{mm\ x}\ \mathbf{1}\boldsymbol{mm}$. The out of plane pitch and yaw motions were accomplished with the help of a Copper wire bonded to the microrobot tip and electrothermal actuator banks to transmit in-plane motion.

Additional refinements to the original AFAM lead to the sAFAM [18, 19], for which we removed the Copper cable transmission, and replaced it with a monolithically fabricated serpentine spring. This design offered many improvements in terms of the fabrication process, assembly, and reliability of operation. These modifications resulted in a reduction of workspace of sAFAM to $\mathbf{16}\boldsymbol{\mu m} \times \mathbf{20}\boldsymbol{\mu m} \times \mathbf{118}\boldsymbol{\mu m}$, with an improvement of resolution and repeatability to $\mathbf{20}\ \boldsymbol{nm}$.

[1] Moath Alqatamin: mhalqa01@louisville.edu

The demonstrated capabilities of the sAFAM in our earlier publications potentially enable realization of the manipulation tasks on nano/microscale. But this particular application requires development of the control solutions allowing precise operation in different environments and at different scales, e.g., during in situ SEM operation or while from the samples are under an optical microscope. In our current version of sAFAM (Figure 1, A) we propose additional design modification to improve accuracy, reliability and to reduce the operation complexity of the overall robot. Here we demonstrate custom control solution allowing remote manipulation of sAFAM by a human operator. Our control system consists of manual controller (joystick), Python based graphic user interface (GUI), and custom control system. Operators can drive the sAFAM with the help of GUI or a programmed gaming Joystick. Based on the direction of joystick motion, a combination of 4 electrothermal actuators will be engaged to drive the sAFAM's end effector in different directions within its workspace. We evaluate the performance of the microrobot tip motions under joystick control in the context of potential future application for nano/micromanipulation tasks.

The reminder of this paper is organized in the following order: in Section 2, we describe our microrobot (design, fabrication, assembly), control system and its tools. In section 3 we present the software implementation for the GUI and joystick control. Then in section 4 and 5 the experimental setup and methods are explained along with the results on joystick resolution and sAFAM displacements and repeatability. Section 6 includes discussion of the experimental results. Finally, we conclude the paper and discuss future work.

2. DESCRIPTION OF SYSTEM HARDWARE

In this section, the design of the hardware setup will be discussed in detail for both the sAFAM microrobot, and its control platform design.

2.1 DESIGN, FABRICATION AND ASSEMBLY of SAFAM

The sAFAM is comprised of two major components: an assembled monolithic arm and the two electrothermal actuator banks arranged in-plane of the die (Figure 1). These two parts are assembled with the help of a MEMS "Zyvex" snap-fastener connectors shown in Figure 2. There are four "chevron" electrothermal actuators (two per each bank) identified as A, B, C, and D, as shown in Figure 1. One thermal actuator consists of two sets of 5 beams attached to the shuttle and anchored by two electrode pads. For example, the actuator A is anchored by pads 2 and 3 (Figure 1). When the thermal actuator is engaged with a voltage, due to Joule-heating, the temperature of the actuator beams increases, resulting in a pushing motiondue to thermal expansion. To achieve the 4 degrees of freedom, the actuation direction of actuators A and C are aligned with the X-axis, while B and D are aligned with the Y-axis. The arm employs a two-spring system to couple the in-plane actuator motion onto its end-effector. The thin beam spring is stiffer along its longitude while softer toward latitude directions. As a result, when actuator A is engaged, the thin beam spring pushes forward and the serpentine spring bends like a pivot to allow the end-effector to generate a downward pitch motion. Similarly, actuator C generates upward pitch motion. B or D individually generates yaw motion towards left or right. Combining A and C generates forward translation, while B, D combination generates leftward translation.

TABLE 1: AFAM/SAFAM DESIGN EVOLUTION (FIGURE 1).

		Microrobot versions		
		AFAM [16,17]	1st version of sAFAM [18,19]	2nd version of sAFAM (this study)
Design Modifications	Length of Robotic arm (cantilever)	1300 μm	2954 μm	3419 μm
	Shuttle (Zyvex micro snap-fastener)	• Spring bank arrangement (passive springs): pair of supporting springs attached to the side of shuttle (Fig 1, B) • Shuttle and shuttle beam connected (Fig 1, B)		• Spring bank arrangement (passive springs): 4 supporting springs attached to each corner of shuttle (Fig 1, C) • Decoupling of shuttle and beam (Fig 1, C)
	Pitch and yaw motion realization	Copper wire assisted motion of the end effector.	Cable removed and motion coupling is realized with monolithic micromachined silicon arm (Fig 1, A).	

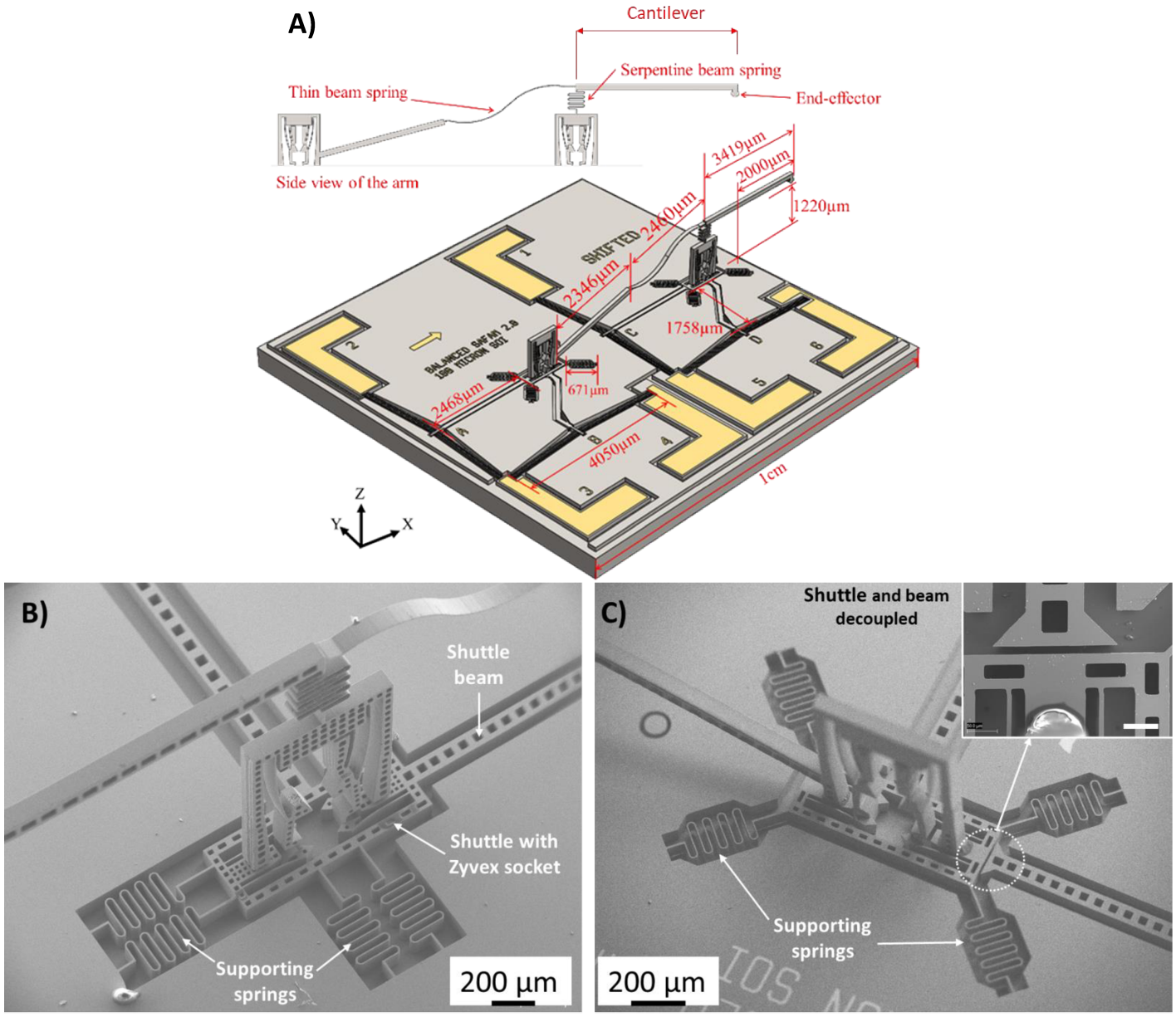

FIGURE 1: A) SAFAM ISO VIEW SOLID MODEL TOP VIEW AND DIMENSIONS OF THE SAFAM'S DESIGN USED IN THIS STUDY, B) SEM IMAGE OF THE SAFAM's COMPONENT – ZYVEX SOCKET AND PLUG (1ST VERSION OF SAFAM), C) SEM IMAGE OF THE 2ND VERSION OF THE SAFAM USED IN THIS STUDY (SCALEBAR IN THE INSET IMAGE – 50 MICRON).

The sAFAM has been continuously developed to function more effectively and accommodate more tasks. In table 1 we present main modifications to the AFAM/sAFAM design. For instance, the current design aims to increase the usable workspace of the end-effector by increasing its reach. To do so, the arm is shifted to be closer to the edge of the die as it shown in Figure 1. The length of the sAFAM's cantilever was also increased, so the end-effector extends from the edge of the die by 2mm. The last change was relocating the supporting springs to each corner of the Zyvex socket rather than in line with the actuators on one side as in the previous designs [19]. This was implemented to better assist the sockets in returning to their original zero position and ensure the stability of the base. Moreover, because the four supporting springs have been moved to the corners, the effect of motion coupling towards Y direction (when engaging actuators A and C individually or combined) is reduced. Static structural simulation conducted in ANSYS confirms such claim, indicating that a 18.93% reduction on Y direction motion coupling when A is engaged alone.

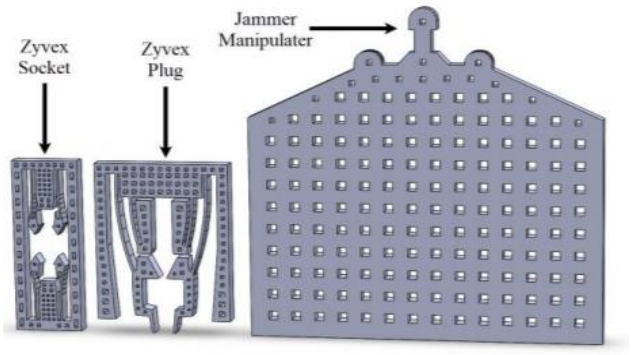

FIGURE 2: ZYVEX SNAP-FASTENER, SOCKET AND TIP JAMMER

sAFAM is fabricated in the cleanroom with standard MEMS fabrication process. It starts with a silicon-on-insulator (SOI) wafer with 100µm device layer with 0.01-0.02 Ohm-cm resistance, 2µm of buried oxide (BOX) layer, and 500µm handle layer. It is cleaned by RCA process to remove any potential contamination and ambient oxidation. Chrome and gold are sputtered under 300W DC sequentially; the chrome promotes adhesion between gold and silicon. The first photolithography defines the pattern of contact pads and the metal are processed by gold and chrome etchant, respectively. The body pattern of the microrobot is defined by the second photolithography process and carved by the subsequent deep reactive ion etching (DRIE) process. Eventually, the wafer is diced, and selected dies are cleaned and released by vapor HF etcher.

The assembly process is performed with our in-house microassembly station NEXUS. It has two sets of motorized stages. A vacuum-secured sample chuck which holds the silicon samples is mounted on top of the first set of manipulators (M_1) with X, Y and θ motion. On the side, the second set of manipulators (M_2) offers motorized X, Y, Z, θ, and manual X, Y motion. To assemble the microrobot, we need another piece – the jammer, which is also fabricated on the same wafer, shown in Figure 2. The jammer is firstly adhered onto M_2, through microscopic vision feedback, the operator aligns the jammer with the Zyvex plug located on the arm and pick it up. Again, the arm is rotated by 90° to be perpendicular to the in-plane thermal actuator socket, then the jammer pushes down the arm and the arm will be temporarily assembled with the thermal actuators. Lastly, we use M_2 to apply UV adhesive to the joints to permanently fix the arm with the thermal actuators. Once the adhesive is cured by UV light, the sAFAM is ready for wire bonding and used.

2.2 POWER SUPPLY AND CONTROLLER

To control the actuation voltage applied to the sAFAM, a control box has been designed and built as shown in Figure 3. It includes a TI USB2ANY interface adapter from Texas Instruments, an Arduino UNO, a development board, a buffer amplifier, and a programmable power supply (RIGOL DP831A). The Arduino serves as a serial translator between the operator's laptop and the

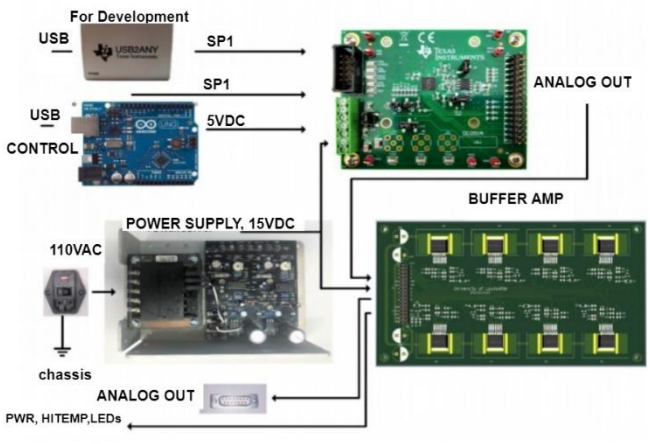

FIGURE 3: BLOCK DIAGRAM OF CONTROL SYSTEM

DAC that is on the development board. The Arduino also limits the voltage allowed to be sent by the operator. The buffer amplifier was originally built to increase the impedance between the control circuit and the sAFAM. Moreover, it is designed to supply +/- 24V.

The Arduino is connected to the user laptop from the back panel of the control box using USB. This allows the operator to use other methods, such as Python, to command voltages to the 7 channels on the front panel. The analog output connection is connected to the six pads of the sAFAM to supply the required voltage to the actuators.

2.3 JOYSTICK

Logitech Flight Simulator Joystick (The Extreme 3D Pro) is used in this development phase of the setup to control the motion of the sAFAM. This joystick has 2 axes that run along a coordinate plane with max values at 1 and minimum values at -1. The sAFAM can move in six different directions but there are only 2 axes on the joystick. A trigger signal is used to switch the control between translational motions (X and Y) and the pitch/ yaw motions. The joystick offers an intuitive control of the sAFAM by applying voltage to its actuators in a precise manner to drive the cantilever by small steps, which makes manipulation of micro-nano scale object less cumbersome.

3. DESCRIPTION OF SYSTEM SOFTWARE

One of the objectives of this work is designing a user-friendly interface to control the sAFAM within its workspace in a precise and accurate way. To achieve that goal, a software based on Python has been developed for both graphical user interface and joystick controller. Figure 4 shows the front panel of GUI. In the upper right, there is a list of the pin connections. Since there are eight channels available on the control box, the operator needs

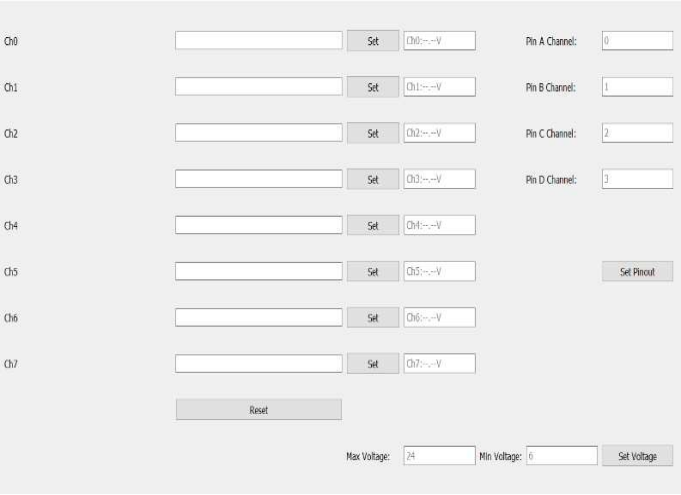

FIGURE 4: FRONT PANEL OF GRAPHICAL USER INTERFACE.

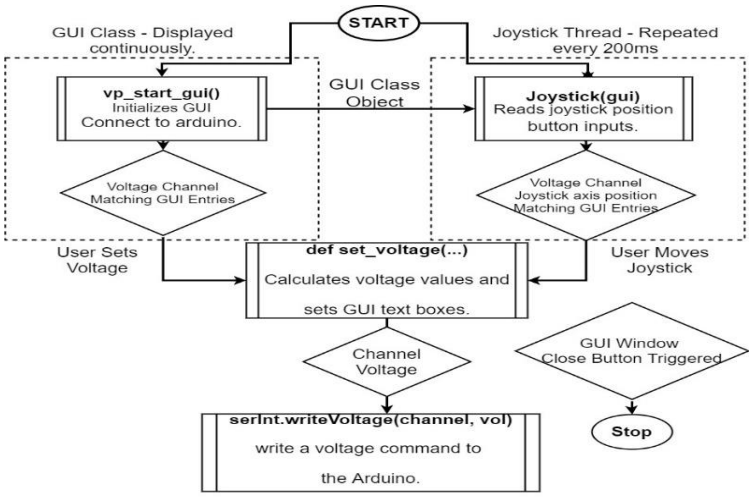

FIGURE 5: CONTROL PROGRAM FLOWCHART FOR GUI AND JOYSTICK.

an option to switch connections to the pads on the sAFAM circuit. The shadow text in the white boxes shows how the program automatically assigns the channels to the pads. Then, on the bottom right, there is an option to change the maximum and minimum allowed voltage the operator can send, either with the joystick or using the GUI. The maximum and minimum voltages required to safely move the sAFAM are different depending on the specific sample as well as environmental condition. This option ensures the flexibility of the controller to use with different sAFM samples. The shadow text displays the max voltage that can be safely produced by the control box and the minimum voltage to cause the arm to move. For instance, they are set to be 24 V and 6V, respectively. This is used to re-adjust the voltage range that is sent by the joystick, to ensure the default is always set to position 1 on the joystick. If the operator chooses to change the maximum voltage to 16 V instead of 24 V, then position 1 of the joystick will follow that flexibility. Another benefit of minimizing the range would be to get better precision with the joystick at the cost of workspace, or to increase the range to increase the workspace at the cost of precision. After the user assigned which channel related to which pad on sAFAM and determine the minimum and maximum voltages, the required voltage can be applied by the set button on the GUI or by moving the joystick. The set voltage function inside the program simply inputs the plain text box for a particular channel selected by the user and converts their string input into a float value. The new float variable is then sent using the serial communication between the operator's laptop and the Arduino. There is also a reset all function that first sets all the channel outputs to zero volts then resets the channel voltage section of the GUI. The reset function runs when the program starts and when the user presses the reset button.

Figure 5 shows the control program flowchart for both the GUI and joystick controller. The user has the option to choose between the GUI and joystick. If the joystick is chosen to control the sAFAM, the program will calculate the required voltage based on the minimum and maximum voltage limits. This voltage is then applied to a specific actuator based on the direction of the joystick movements.

4. EXPERIMENTAL SETUP

Figure 6 shows the experimental setup to evaluate the performance of the sAFAM as well as its control interfaces. The control box and joystick are connected to the user's laptop via USB port. The sAFAM was wired to the control box and placed on a microscope attached to two cameras. These two cameras (Edmund EO-3112C) capture images in both horizontal and vertical views for the sAFAM displacements in XY and Z directions. The embedded grid feature of these cameras allows movements of object under microscope as small as six microns. The acquired images from the camera are processed to extract the displacements of the sAFAM end effector. A conversion factor (C) is used to convert the pixel information into their equivalent displacement by using micron scale. This conversion factor can be calculated by taking an image of micron scale at the same magnification and image settings of the displacement images.

Once the conversion factor is determined, the following procedure is followed to calculate the tip displacement in micron. First, the zero-position image of the arm tip is uploaded to ImageJ. Then, a line is drawn that crossed from the dark background to a much lighter sAFAM arm. The starting position of the line drawn and the point on the graph where the contrast changed drastically was recorded. After that, a new line is drawn on the actuated image that started at the same pixel position as the zero position. Again, the point of contrast change was recorded and the difference between the two contrast points was calculated. Figure 7 shows the pixel difference and contrast relationship for an actuated arm of sAFAM. From the figure, the displacement of the sAFAM arm in micron ($\Delta d_{\mu m}$) is calculated by

$$\Delta d_{\mu m} = C \Delta d_{pixel} \quad (1)$$

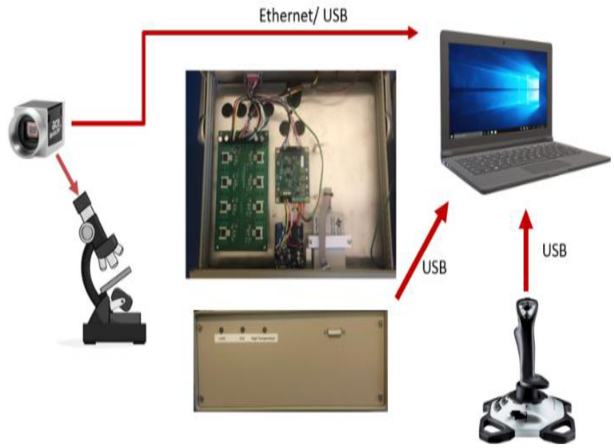

(A)

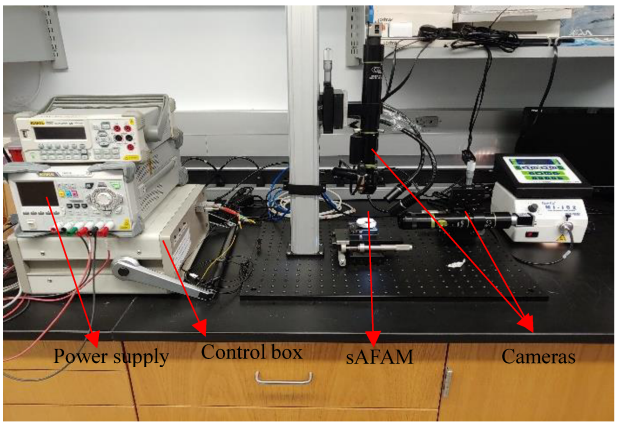

(B)

FIGURE 6: (A) BLOCK DIAGRAM OF EXPERIMENTAL SETUP **(B)** EXPERIMENTAL SETUP.

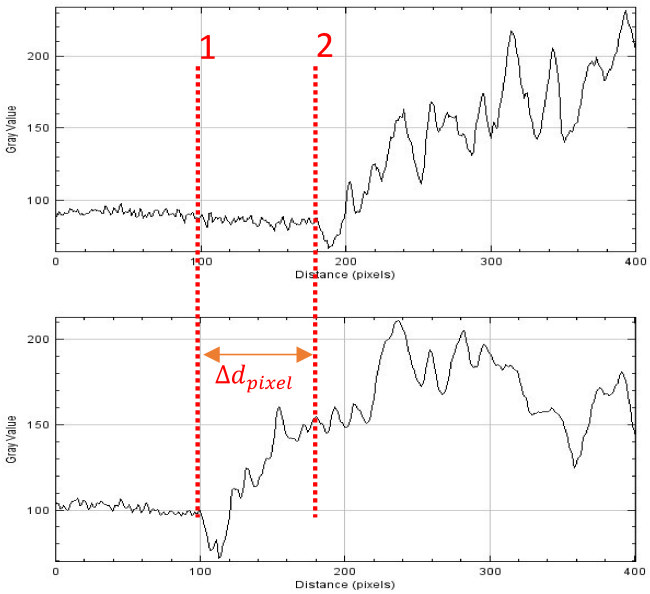

FIGURE 7: PIXEL DIFFERENCE CALCULATION IN IMAGEJ SOFTWARE.

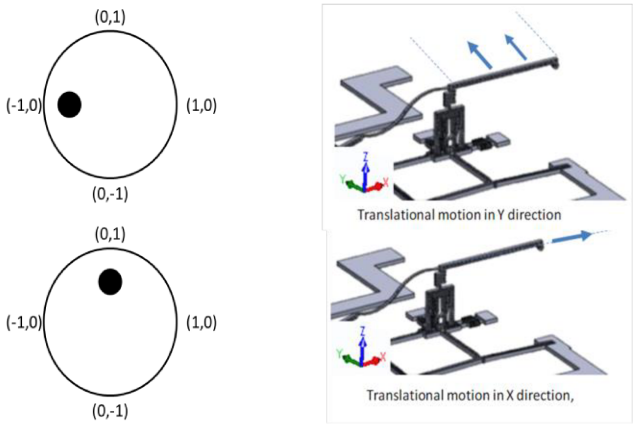

(A)

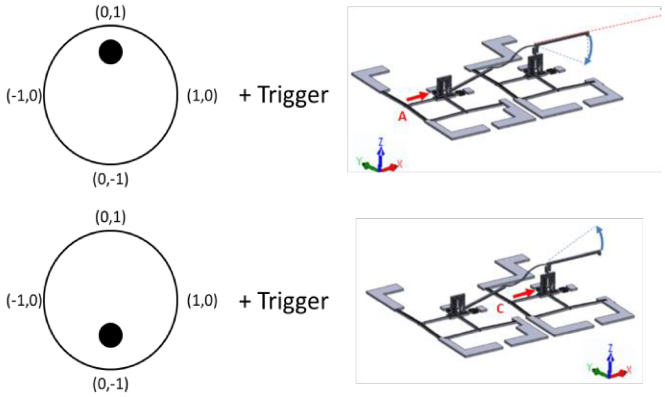

(B)

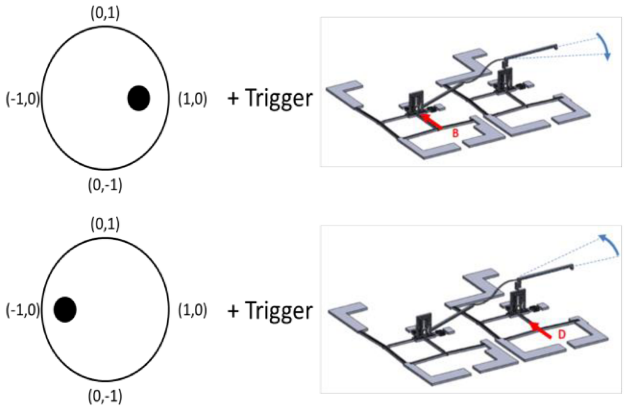

(C)

FIGURE 8: SAFAM'S END-EFFECTOR TRAJECTORIES (RIGHT-SIDE), CORRESPONDING TO THE DIRECTIONAL MANIPULATION OF THE JOYSTICK (LEFT SIDE). (A) XY TRANSLATIONAL MOTIONS (B) PITCH MOTION IN Z DIRECTION (C) YAW MOTION IN THE XY PLANE.

5. RESULTS

5.1 JOYSTICK TELEOPERATION OF SAFAM

The joystick controller is used to apply voltage to a specific actuator of the sAFAM. Figure 8A shows that to realize translational motion of end effector in X direction, the same voltage should be applied to both actuators A and C. For translational Y direction movement, the voltage must be applied to B and D simultaneously (Figure 8A). Moreover, a voltage that applied to A or C will introduce a pitch motion in Z direction (Figure 8B). Yaw motion of the arm in the XY plane can be realized by engaging either B or D actuators (Figure 8C).

In the Figure 9 is depicted shows the relationship between the joystick movements and the output voltage that applied to the sAFAM actuators. We can see that the joystick resolution is around 3V per movement above the minimum voltage which is 6 V in this case.

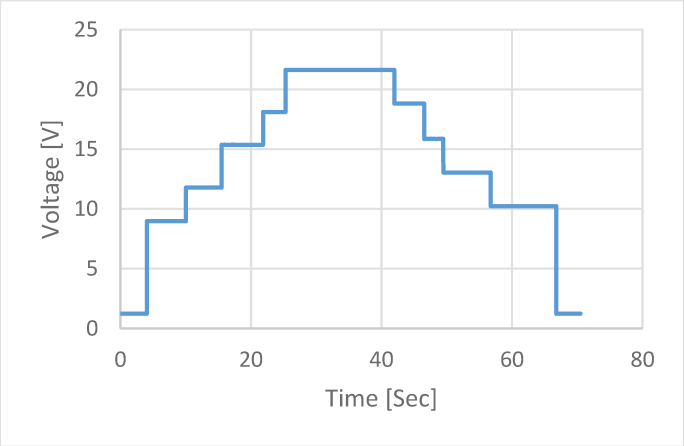

FIGURE 9: JOYSTICK OUTPUT VOLTAGE RELATED TO JOYSTICK MOVEMENTS FOR CHANNEL A.

5.2 EXPERIMENTAL RESULTS – SAFAM DISPLACEMENT

Figure 10 shows an example of the images from the microscope that used to calculate the displacement in Y direction. A voltage of 22 V is applied into actuators B and D by moving the joystick to the left direction as shown in Figure 8A. Using Figure 10 and calculated conversion factor, the average displacement of ten measurements is calculated to be 4.04 μm. Figure 11 shows the displacement of the cantilever in Z direction (Pitch up) after applying a 22 V on C actuator only (See Figure 8B for the joystick motion direction). The average displacement is around 47.92 μm.

Table 1 summarizes the average displacement in XYZ directions for ten trials. To test the resolution of the proposed joystick controller, an operator moves the joystick with a lowest possible force to apply minimum voltage and records the corresponding displacement. The resolution in the Z direction for both pitch up and down are calculated to be 8.4μm and 7.3μm respectively. The minimum displacements in all directions are summarized in Table 1.

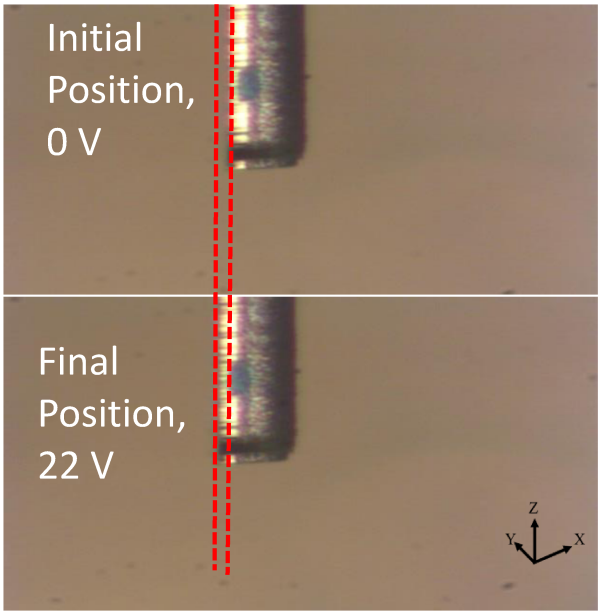

FIGURE 10: TWO PICTURES FOR Y DIRECTION DISPLACEMENT BY APPLYING 22V AT BD ACTUATORS

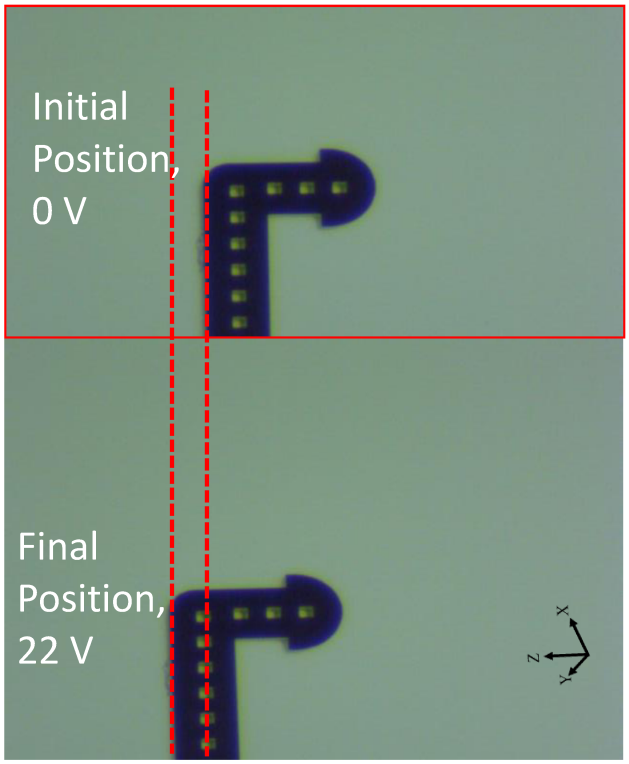

FIGURE 11: TWO PICTURES FOR Z DIRECTION DISPLACMENT (PITCH UP) BY APPLYING 22V TO C ACTUATOR.

TABLE 1: AVERAGE DISPLACEMENTS OF SAFAM AND STANDARD DEVIATION σ FOR TEN MEASUREMENTS

		Parameters			
		Act.	Displacement, μm (mrad)		σ, μm (mrad)
			Max	Min	
Motion Direction	Transl. (X)	AC	6.09	2.9	0.33
	Transl. (Y)	BD	4.10	0.91	1.45
	Pitch Up (Z^+)	C	47.92 (13.7)	8.4 (2.4)	1.17 (0.3)
	Pitch Down (Z^-)	A	63.41 (18.1)	7.3 (2.1)	0.91 (0.3)
	Yaw (XY^-)	D	23.19 (3.9)	5.6 (0.9)	1.67 (0.3)
	Yaw (XY^+)	B	8.44 (2.4)	1.1 (0.3)	1.05 (0.3)

TABLE 2: REPEATABILITY OF SAFAM END EFFECTOR FOR MAXIMUM DISPLACEMENT (10 REPETITIONS).

		Actuators	Repeatability, μm (mrad)
Motion Direction	Translation (X)	AC	0.7
	Translation (Y)	BD	2.75
	Pitch Up (Z^+)	C	3.15 (0.7)
	Pitch Down (Z^-)	A	2.46 (0.6)
	Yaw (XY^-)	D	3.85 (0.6)
	Yaw(XY^+)	B	2.11 (0.6)

An important factor to evaluate a manually controlled microscale robotic system is a correspondence between the joystick operator inputs and resulting motion of the sAFAMS robotic arm. In this experiment microrobot's end effector was moved by operator from initial to maximum position and then back to the initial. Displacement of the sAFAM's arm was measured with the help of a Keyence laser displacements sensor (LK-G5000, Keyence Corporation, IL, USA). Figures 12 presents the results of the measured joystick controller voltage (top black line) and corresponding motion of the sAFAM's end effector (bottom blue line). Figure 12 A illustrates change of the joystick's voltage directed to the sAFAM's actuator B resulting in yaw motion of the end effector and Figure 12 B illustrates changes of the voltage directed to the actuator A and respective pitch motion of the sAFAM's arm.

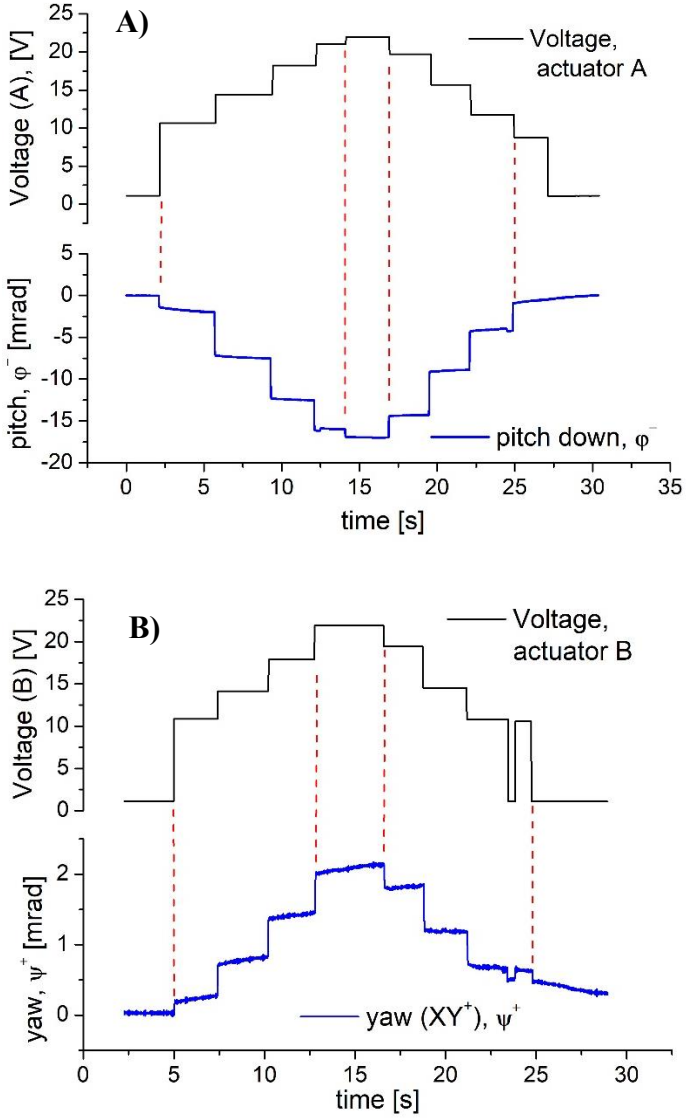

FIGURE 12: JOYSTICK VOLTAGE OUTPUT CORRESPONDING TO SPECIFIC MOTION OF THE sAFAM'S END EFFECTOR: A) PITCH MOTION OF END EFFECTOR GENERATED BY ENGAING ACTUATOR A; B) YAW MOTION OF END EFFECTOR – ACTUATOR A.

Repeatability is a performance criterion that primarily determines the applicability of these types of microrobots. It is defined here as the number of times a robotic arm returns to its original location after N times operation for the same operating task. Table 2 summarizes the repeatability of the sAFAM end effector for X, Y and Z directions for ten experiments by moving the joystick to the same position each time. The joystick is moved to the maximum range to make sure that the same voltage is applied in each experiment.

6. DISCUSSION

Performance of the sAFAM, in terms of displacement is primarily affected by the structural properties of the microrobot and motion translation from the given actuator to the robotic arm [16-19]. It is evident from the data presented in table 2 that workspace of our microrobot is significantly reduced compare to its previous versions resulting in6 micron towards X, 4 micron towards Y and smaller displacement values of pitch and yaw motion. The most likely reason is decoupling of the shutter and the beam which affected efficient translation of the motion under the actuator (via shuttle beam) to the shuttle with Zyvex socket. In a result the observable motion of the end effector under OM is accomplished for minimum voltage of approximately 7 V. Standard deviation values indicate that the best performance of sAFAM is realized for the motion driven by the A and C actuators (Table 1) which is consistent with repeatability values (Table 2). Relatively high values of the st. deviation and repeatability could be partially due to the adopted measurement method utilizing the microscope camera. For a given magnification camera's resolution and consequently pixel size will always be an inherent limitation for the precise determination of the displacement. Nevertheless, considering that our conversion factor in this study was usually below one micron for given magnification, measurement method is definitely not the main contributing factor.

Operator induced errors are another source of uncertainty for manually controlled robotic system like sAFAM, that affects the reliability and precision of the end effector motion. It is evident from the figure 12 that discrete changes of the voltage (steps) are not constant which is caused due to operator's inability to precisely control the inputs using joystick. Any minor hesitation by operator during joystick operation resulted in the fluctuation of motion of the sAFAM's end effector. Figure 12 A (close to 25th second) shows such a change in the end effector's position.

Lastly, performance of the sAFAM (repeatability with respect to the displacement) is modest when compared to other commercially available tools for nano/micromanipulation [1,2] which are based on the piezoelectric actuators with resolution and repeatability much better [1]. Nevertheless, sAFAM could be still a cost-effective tool with specific advantages over the commercial probing devices. Firstly, because of the lower manufacturing costs. Secondly, sAFAM could be considered as a highly specialized instrument for unique applications where high performance is not necessary and due to space limitations piezoelectric devices would not be practical. In order to achieve this, it is critical to improve performance of our microrobot as we plan further development of sAFAM., Also unique design and specialization of our tool makes it hard to compare to other custom MEMS based probing tools in development [2, 12, 13]. Overall, our results indicate that we were able successfully realize 4 DOF motion of microrobot with the help of the low-cost custom control system utilizing joystick (Table 2, 3, Figure 11, 12).

7. CONCLUSION

A modified design of an Articulated Four Axes Microrobot (sAFAM) is introduced to improve its performance and stability. Both hardware and software control platform has been designed for controlling the sAFAM in a three-dimensional workspace. A graphical user interface (GUI) and a gaming joystick controls are implemented by using Python programming language. The performance and repeatability of the end effector of the sAFAM are then evaluated by using both the joystick controller and the GUI interface. Experimental results of end effector motion in six different axes, from 10 repeated measurement indicates a moderate repeatability of resulting motion, with a minimum standard deviation value of 0.33 μm in X axis and a maximum value of 1.67 μm in Yaw (XY^{-}) axis. In future we will improve the controller of the sAFAM to minimize human induced errors during microrobot operation, enhance its precision metrics, and test it for in situ SEM nano/microscale manipulation.

ACKNOWLEDGEMENTS

This research was supported by the National Science Foundation awards EPSCOR- KAMPERS #1849213 and NRI project # 1734383.

REFERENCES

[1] S. Mekid and S. Bashmal, "Engineering manipulation at nanoscale: further functionalspecifications", Journal of Engineering, Design and Technology, Vol. 17, No. 3, pp 572-590, 1726-0531, 2019

[2] C. Jiang, H. Lu, H. Zhang, Y. Shen, and Y. Lu, " Recent Advances on In Situ SEM Mechanical and Electrical Characterization of Low-Dimensional Nanomaterials ", Scanning, Vol. 2017, 1985149, 2017.

[3] Z. Yang, A. Sherehiy, S. S. Chowdhury, D. Wei, R. Zhang, and D. O. Popa, "Design, Fabrication and Experimental Validation of a Steerable, Laser-Driven Microrobot in Dry Environments," in *2020 IEEE 16th International Conference on Automation Science and Engineering (CASE)*, 20-21 Aug. 2020 2020, pp. 882-887, doi: 10.1109/CASE48305.2020.9216958.

[4] S. S. Chowdhury, Z. Yang, A. Sherehiy, D. Wei, R. Zhang, and D. O. Popa, "Parametric Investigation of Laser-Driven Microrobot Manoeuvrability on Dry Substrates " in *2020 International Conference on Manipulation, Automation and Robotics at Small Scales (MARSS)*, 2020.

[5] J. F. Klotz *et al.*, "Concept Validation for a Novel Stick-and-Slip, Light-Powered, Mobile Micro-Crawler," in *2019 International Conference on Manipulation, Automation and Robotics at Small Scales (MARSS)*, 1-5 July 2019 2019, pp. 1-7, doi: 10.1109/MARSS.2019.8860938.

[6] R. Zhang, A. Sherehiy, Z. Yang, D. Wei, C. K. Harnett, and D. O. Popa, "ChevBot – An Untethered Microrobot Powered by Laser for Microfactory Applications," in *2019 International Conference on Robotics and Automation (ICRA)*, 20-24 May 2019 2019, pp. 231-236, doi: 10.1109/ICRA.2019.8793856.

[7] F. Soto, E. Karshalev, F. Zhang, B. Esteban Fernandez de Avila, A. Nourhani, and J. Wang, "Smart Materials for Microrobots," *Chemical Reviews,* 2021/02/01 2021, doi: 10.1021/acs.chemrev.0c00999.

[8] M. Gauthier, E. Gibeau, and D. Heriban, "Submerged Robotic Micromanipulation and Dielectrophoretic Micro-object Release," in *2006 9th International Conference on Control, Automation, Robotics and Vision*, 5-8 Dec. 2006 2006, pp. 1-6, doi: 10.1109/ICARCV.2006.345273.

[9] S. Fatikow, J. Seyfried, S. Fahlbusch, A. Buerkle, and F. Schmoeckel, "A flexible microrobot-based microassembly station," in *1999 7th IEEE International Conference on Emerging Technologies and Factory Automation. Proceedings ETFA '99 (Cat. No.99TH8467)*, 18-21 Oct. 1999 1999, vol. 1, pp. 397-406 vol.1, doi: 10.1109/ETFA.1999.815384.

[10] R. Yeh, E. J. J. Kruglick, and K. S. J. Pister, "Microelectromechanical Components For Articulated Microrobots," in *Proceedings of the International Solid-State Sensors and Actuators Conference - TRANSDUCERS '95*, 25-29 June 1995 1995, vol. 2, pp. 346-349, doi: 10.1109/SENSOR.1995.721817.

[11] N. Sarkar, D. Strathearn, G. Lee, M. Olfat, and R. R. Mansour, "A platform technology for metrology, manipulation and automation at the nanoscale," in *2017 International Conference on Manipulation, Automation and Robotics at Small Scales (MARSS)*, 17-21 July 2017 2017, pp. 1-6, doi: 10.1109/MARSS.2017.8001949.

[12] S. Bhowmick, D. Stauffer, H. Guo, S. Kaps, Y.K. Mishra, V. Hrkac, O. Warren, R. Adelung, A. Minor, and L. Kienle, " In Situ Electromechanical Study of ZnO Nanowires", Microscopy and Microanalysis , Volume 19 , Issue S2: Proceedings of Microscopy & Microanalysis 2013 , August 2013 , pp. 434 - 435

[13] Z.Gong; B. K. Chen; J. Liu; Y. Sun, "Robotic Probing of Nanostructures inside Scanning Electron Microscopy", IEEE Transactions on Robotics, Vol. 30, Issue: 3, June 2014

[14] T. K. a. G. A, "Sockets for microassembly," United States Patent US7025619B2, 2004.

[15] S. G. a. T. K. Geisberger A, "Microconnectors and non-powered microassembly therewith," United States Patent patent EP1564183A2, 13/2/2004.

[16] R. Murthy and D. O. Popa, "A four degree of freedom microrobot with large work volume," in *2009 IEEE International Conference on Robotics and Automation*, 12-17 May 2009 2009, pp. 1028-1033, doi: 10.1109/ROBOT.2009.5152812.

[17] R. Murthy, H. E. Stephanou, and D. O. Popa, "AFAM: An Articulated Four Axes Microrobot for Nanoscale Applications," *IEEE Transactions on Automation Science and Engineering,* vol. 10, no. 2, pp. 276-284, 2013, doi: 10.1109/TASE.2012.2217740.

[18] R. Zhang, D. Wei, and D. O. Popa, "Design, Analysis and Fabrication of sAFAM, a 4 DoF Assembled Microrobot," in *2018 International Conference on Manipulation, Automation and Robotics at Small Scales (MARSS)*, 4-8 July 2018 2018, pp. 1-6, doi: 10.1109/MARSS.2018.8481182.

[19] R. Zhang, A. Sherehiy, D. Wei, and D. O. Popa, "Design and characterization of solid articulated four axes microrobot for microfactory applications," *Journal of Micro-Bio Robotics,* vol. 15, no. 2, pp. 119-131, 2019/12/01 2019, doi: 10.1007/s12213-019-00118-y.